

CAP-Net: Correspondence-Aware Point-view Fusion Network for 3D Shape Analysis

Xinwei He^{1*} Silin Cheng^{1*} Song Bai² Xiang Bai^{1†}

¹Huazhong University of Science and Technology

²Bytedance Research

{eriche.hust, songbai.site}@gmail.com {slcheng,xbai}@hust.edu.cn

Abstract

Learning 3D representations by fusing point cloud and multi-view data has been proven to be fairly effective. While prior works typically focus on exploiting global features of the two modalities, in this paper we argue that more discriminative features can be derived by modeling “where to fuse”. To investigate this, we propose a novel Correspondence-Aware Point-view Fusion Net (CAP-Net). The core element of CAP-Net is a module named Correspondence-Aware Fusion (CAF) which integrates the local features of the two modalities based on their correspondence scores. We further propose to filter out correspondence scores with low values to obtain salient local correspondences, which reduces redundancy for the fusion process. In our CAP-Net, we utilize the CAF modules to fuse the multi-scale features of the two modalities both bidirectionally and hierarchically in order to obtain more informative features. Comprehensive evaluations on popular 3D shape benchmarks covering 3D object classification and retrieval show the superiority of the proposed framework.

1. Introduction

3D object recognition is undoubtedly an important research topic in computer vision and has drawn increasing attentions due to its essential role in a wide range of applications such as autonomous driving, virtual reality (VR), and 3D printing. Recently, it has become a dominant direction to apply the powerful deep neural networks to learn representations from these 3D data automatically for recognition. Given a 3D object, various raw data formats (or modalities) can be employed to model it, *e.g.*, point clouds, multiple views, or voxels. Most existing works focus on learning to extract representations from only one modality, such as MVCNN [36] working on multiple views, PointNet [31]

working on point cloud data, and VoxelNet [28] working on voxels. These unimodal methods which adapt to a single modality of a 3D object have led to impressive progress.

However, different modalities have different, and usually complementary capacities to represent 3D objects. For instance, voxels and point clouds can capture the geometry information of 3D objects, while projected views are easier to obtain due to the ubiquitous 2D cameras in daily life and more well-engineered 2D convolutional networks can be used. It motivates us to investigate solutions to fuse representations from multiple modalities. In this paper, we follow previous works [47, 48] and choose to fuse point cloud and multi-view data since these two modalities are direct outputs of 2D and 3D acquisition devices. Besides, voxels are sparse representations of 3D objects and generally consume more memory.

Existing works on fusion of point cloud and multi-view images have demonstrated that by considering the relative correlations of the two-modal data, more discriminative 3D representations for recognition can be derived. The pioneering work PVNet [47] exploits the relative correlations between the global multi-view features and the local features of point cloud. PVRNet [48] further explores the benefits of learning the relations between global features of each view and point cloud. Although these works have obtained promising results, they still do not fully take advantage of the local spatial relations between the two-modal data, which are potentially helpful to improve the capacity of the fused representations.

In this paper, we introduce a novel framework named Correspondence-Aware Point-view Fusion Net (CAP-Net) to fuse point cloud and multi-view data by fully exploiting the local cross-modal correspondence (or relations). Particularly, the network adopts a module named Correspondence-Aware Fusion (CAF) and applies it to fuse the multi-scale features of the two-modalities in a hierarchical manner. Unlike previous works [47, 48], The CAF module selectively picks corresponding local cues from one modality to enhance the relevant local representations from

*indicates equal contributions.

†Corresponding author.

the other modality. Inspired by self-attention [37], the cross-modal correspondence scores between all the possible local region pairs are first estimated. Then the scores with smaller values are filtered out to reduce the redundancy and thus obtain more complementary features. Based on them, the model learns to produce more discriminative representations.

One important characteristic of the CAP-Net is that it fuses the point cloud and multi-view data in a bidirectional manner. It can be easily achieved by adopting two CAFs at each scale and selects one modality as the query to be enhanced alternately, and use the remain modality to provide local cues for the query. Such a bidirectional way can ensure that each modality contributes to the final combined representations in a more interactive and comprehensive manner. Our CAP-Net which is aware of “where” to fuse is very effective in combining representations of multi-view images and point clouds. As shown in Fig. 1, it succeeds to incorporate the most relevant local features from the four views to enhance the four selected point features for an airplane object. Another notable merit of the proposed CAP-Net is that it is highly parameter-efficient, which has $2.8\times$ fewer parameters than the prior state-of-the-art work PVRNet [48]. However, encouragingly, when compared with it, we still improve the performance on the ModelNet40 dataset by 2.4% and 0.6% in mean Average Precision (mAP) and Overall Accuracy (OA), respectively.

To summarize, the main contributions of this work are the following:

- We propose a novel module named Correspondence-Aware Fusion (CAF) to fuse representations of point cloud and multi-view data by leveraging their local spatial correspondence scores which are thresholded to obtain stable complementary local features and reduce redundancy.
- Based on the CAF module, we present a framework named Correspondence-Aware Point-view Fusion Net (CAP-Net) to fuse multi-scale representations of the two modalities both bidirectionally and hierarchically, which can mine rich cross-modal corresponding relations, producing more expressive features.
- We conduct extensive experiments to analyze the proposed approach and achieve significant improvements over state-of-the-art methods on the ModelNet40 and ModelNet10 datasets.

2. Related Work

A large body of work has been proposed over the last three decades to address the problem of extracting 3D shape descriptors [33, 19, 5, 20, 22, 1, 2, 8, 3, 50, 16, 10]. In this

section, we briefly review some recent data-driven based 3D representation learning methods. Generally speaking, these works can be coarsely divided into two categories: unimodal based methods and multi-modal based methods.

Unimodal based Methods. For unimodal based methods [18, 35, 34, 25, 31, 28, 41, 27, 7, 46], they focus on learning discriminative representations from one single modality of 3D objects. The modality is often chosen among multi-view images, point clouds, voxels or even meshes. Different modalities face different design problems on the frameworks adopted. The pioneering work on learning representations from multi-view images is MVCNN [36]. It firstly uses one CNN to extract the features for each view image, and then performs view-pooling to aggregate a compact representation. Finally, it feeds the aggregated feature into another CNN for label prediction. However, the view-pooling layer in the MVCNN may induce information loss, especially the spatial dependency. To remedy this, a lot of following works [38, 49, 11, 23, 43, 13, 15] have been proposed. For instance, Siamese CNN LSTM [6] uses Long-Short Term Memory to aggregate the features. With respect to learning from voxels, VoxNet [28] uses 3D convolutional neural networks to achieve this goal. However, since the voxel grid is memory-consuming, these methods are generally limited to low resolution (*e.g.*, voxel grid of 30^3). The following work OCNN [39] proposes to use octree data structure, however, it still requires a serious overhead. PointNet [31] is the first approach that successfully learns representations from point clouds. It uses fully-connected layers to embed the point coordinates and then pools the point-wise features together. However, it does not consider each point’s local neighborhood. To address this issue, a series of works have been proposed [32, 51, 24, 42, 45, 44]. In [40], EdgeConv is proposed to extract local features by connecting each centroid with its k -nearest neighbors. RSCNN [26] proposes a new convolution operator which aims to exploit the geometric relation of points. Recently, several works [9, 14] learn 3D representations directly from meshes, and obtain promising results.

Multi-Modal based Methods. Multi-modal based methods exploit two or more modalities of 3D objects, and learn to fuse them into more discriminative representations. The idea behind is that different modalities may provide different aspects of 3D objects, and they are complementary and can be fused together to enhance the feature learning process. FusionNet [17] learns to combine representations from the volumetric and multi-view data, which brings significant improvements on 3D object recognition task. PVNet [47] focuses on integrating global features from multi-view images with the local features from point cloud. The following work PVRNet [48] introduces a relation score module to exploit the relationship between the

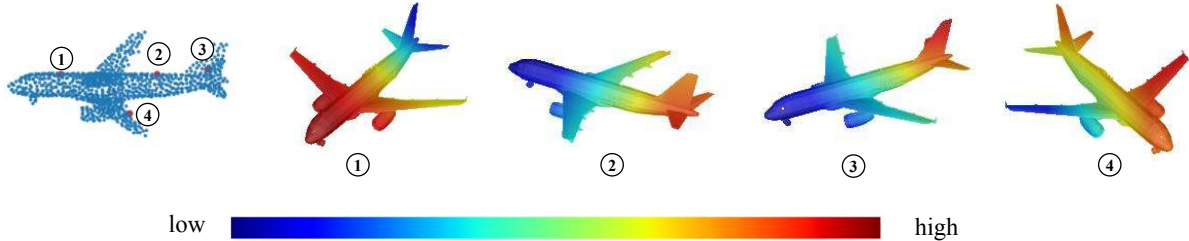


Figure 1. Visualization of the local cross-modal correspondence scores learned by the proposed model. Four points from the point cloud (the first column) and their correspondence scores with four view images (the right three columns) are shown

point cloud and each view image. MMJN [30] improves the performance by fusing panoramic view, the multi-view images and point cloud together. Shape Unicode [29] learns to combine representations of voxel, point cloud, and multi-view images.

3. Approach

Let $\mathcal{D} = \{(\mathcal{O}_i, y_i)\}_{i=1}^{N_o}$ denote the training set consisting of N_o 3D objects, where \mathcal{O}_i represents the i -th 3D object and y_i represents the associated category taking a value from a predefined label set. Without loss of generality, we discard the subscript i for simplicity. For each 3D object \mathcal{O} , N_v view images $\{v^j\}_{j=1}^{N_v}$ are projected and N_p points $\{p_m\}_{m=1}^{N_p}$ are uniformly sampled from the surface to describe it, where v^j represents the j -th projected view and $p_m \in \mathbb{R}^3$ represents the m -th point with the 3D coordinates as its raw feature. The goal of this work is to fuse representations of the two modalities (*i.e.*, multi-view and point cloud) into a compact and discriminative one for 3D object recognition. To achieve this goal, we propose a simple and efficient framework named CAP-Net to fuse the two-modal inputs by leveraging their local spatial relations both hierarchically and bidirectionally. Fig. 2 illustrates the overview of the proposed CAP-Net. In essence, it can be decomposed into four stages. The first two stages involve extracting multi-scale features for the multi-view images and point clouds, respectively. The third stage, which is the core part of our CAP-Net, aims at fusing the two-modal representations at each scale based on the proposed CAF module. The details of the module is elaborated in subsection 3.2. Finally, the fused representations of each scale, the global point cloud and multi-view features are combined together and fed into fully-connected layers for label prediction.

3.1. Extracting Multi-scale View and Point Cloud Features

Extracting Multi-scale View Features. Given multi-view images of a 3D object \mathcal{O} , we first use the convolutional layers of AlexNet [21] (denoted as Alex-Conv) to extract representations for each view. In particular, for the j -th view image v^j , the Alex-Conv outputs convolutional feature map

$\mathbf{F}_v^j \in \mathbb{R}^{c \times h \times w}$, where c , h and w represent the channel size, the spatial height and width of the feature map, respectively. Based on it, we further apply L convolutional layers to it, which reduce the resolution of the feature map \mathbf{F}_v^j progressively and give us a hierarchy of features, denoted by $\{\mathbf{F}_{v,1}^j, \mathbf{F}_{v,2}^j, \dots, \mathbf{F}_{v,L}^j\}$. We further pack representations of the same scale from the multi-views together and perform view-pooling (*i.e.*, max-pooling) to get a compact representation for each scale l :

$$\mathbf{F}_{v,l} = \max\text{-pool}(\mathbf{F}_{v,1}^l, \mathbf{F}_{v,2}^l, \dots, \mathbf{F}_{v,L}^l). \quad (1)$$

where $l \in \{1, 2, \dots, L\}$. It should be noted that the feature vector at each pixel position in the feature map $\mathbf{F}_{v,l} \in \mathbb{R}^{c_v^l \times h_v^l \times w_v^l}$ gives us the most discriminative region descriptor within multi-view images. In our method, we only use three convolutional layers (*i.e.*, $L = 3$) for resolution reduction without changing the channel size (*i.e.*, $c_v^1 = c_v^2 = c_v^3 = D$). For ease of interpretation, the convolutional feature map for each scale l is further flattened along the last two dimensions, producing $\mathbf{F}_{v,l} = [\mathbf{f}_{v,l,1}, \mathbf{f}_{v,l,2}, \dots, \mathbf{f}_{v,l,t}, \dots, \mathbf{f}_{v,l,w_v^l h_v^l}]$, where $\mathbf{f}_{v,l,t} \in \mathbb{R}^{c_v^l}$.

Extracting Multi-scale Point Features. We adopt the Edge-Conv layers of DGCNN [40] (denoted as DGCNN-EConv) as the base feature extractor for the point cloud. Given the 3D point cloud $\{p_m\}_{m=1}^{N_p}$, DGCNN-EConv outputs the corresponding point-wise features $\mathbf{F}_p = \{\mathbf{f}_{p_m}\}_{m=1}^{N_p}$, where $\mathbf{f}_{p_m} \in \mathbb{R}^D$ represents feature vector for point p_m which is computed by aggregating its local contextual neighbors. In order to abstract the local points, we are inspired by PointNet++ [32] and design a module named Sample and Group Pooling (SGP) to perform down-sampling and feature aggregation over it. As shown in Fig. 3(a), it first down-samples the point cloud using Furthest Point Sampling (FPS) to select N_q center points. Then, for each center point p_{c_r} , it mines the k -nearest neighbors $\{p_{r_1}, p_{r_2}, \dots, p_{r_k}\}$ to construct the local spatial context for it. Finally it updates the center point features by applying max-pooling to the features of its nearest neighbor:

$$\mathbf{f}_{p_{c_r}} = \max\text{-pool}(\mathbf{f}_{p_{r_1}}, \mathbf{f}_{p_{r_2}}, \dots, \mathbf{f}_{p_{r_k}}). \quad (2)$$

In this way, we obtain a subsampled point set with N_q

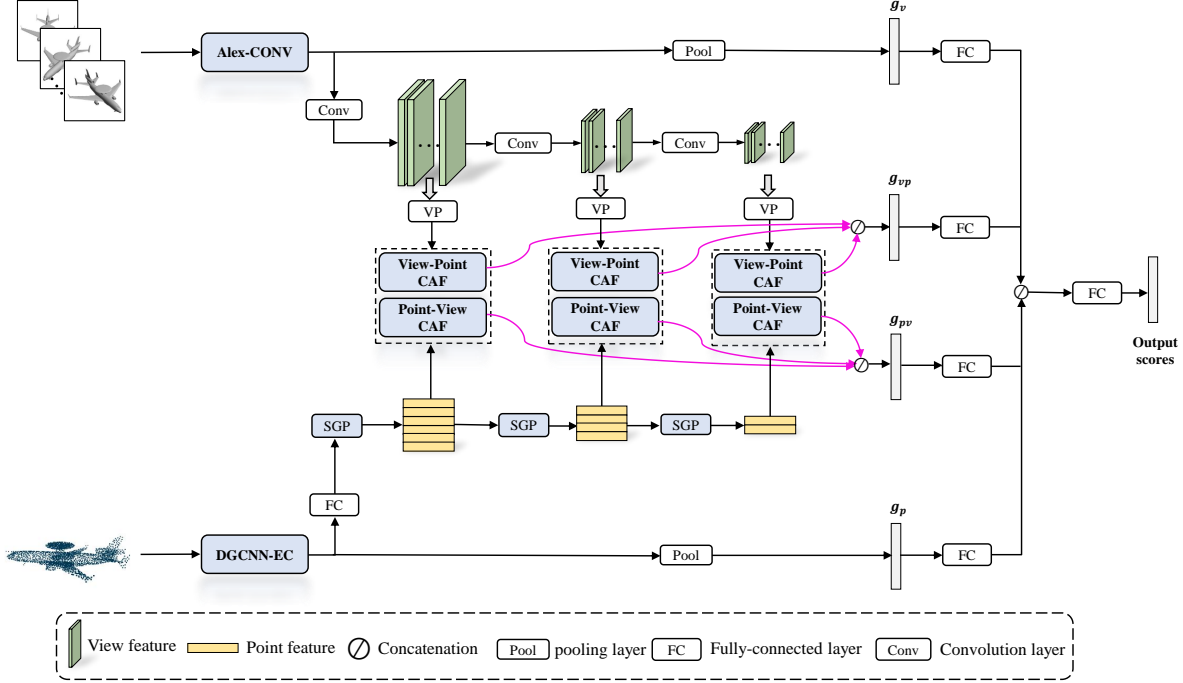


Figure 2. Overview of CAP-Net. The Point-View CAF and View-Point CAF are both based on the CAF module (see subsection 3.2). While Point-View CAF module enhances the point features by the multi-view features, the View-Point CAF enhances the multi-view features by the point features

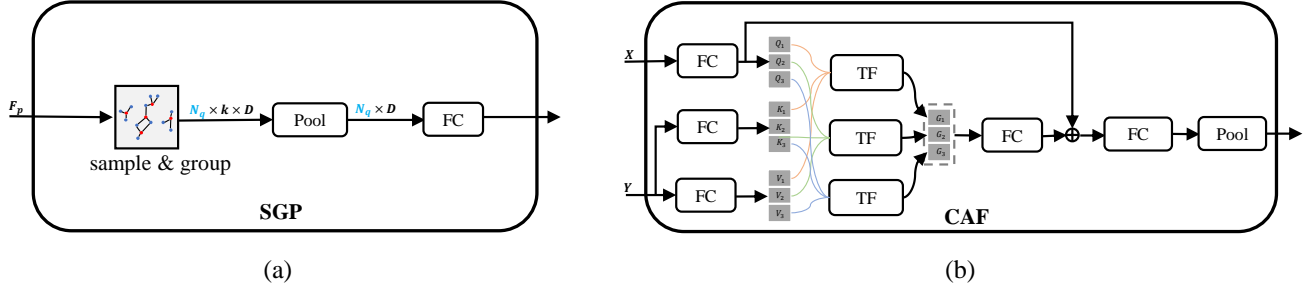


Figure 3. Structures of (a) Sample and Group Pooling (SGP) module and (b) Correspondence-Aware Fusion (CAF) module. Within CAF, TF represents the threshold fusion head which is defined in subsection 3.2. For ease of illustration, the number of TFs or heads (*i.e.*, H) is set to 3

points and their corresponding features $\mathbf{F}_{p,1} = \{\mathbf{f}_{c_z}\}_{z=1}^{N_q}$. One fully connected layer is further used to embed them. It should be noted that each center point features can be viewed as descriptor for a local region of the original point cloud at some scale. In our approach, we use the **SGP** module L times sequentially in order to obtain multi-scale representations of the point cloud, which give us $\mathbf{F}_{p,1}, \mathbf{F}_{p,2}, \dots, \mathbf{F}_{p,L}$ respectively. We denote the obtained point numbers in the L stages as $N_{q,1} \dots, N_{q,L}$. Empirically, the point numbers are decreased by a factor of 2 at each stage in order to obtain multi-scale point features.

3.2. Fusing Multi-view and Point Cloud Features

After obtaining the multi-scale representations for point cloud and multi-view images, we then propose to fuse the two-modal representations by leveraging their rich local relations. Compared with previous methods [47, 48] which use the global view features or global point features for fusion, fusing the local features by exploiting their relevance or correspondence scores allows us to adaptively collect discriminative cues from each modality to learn more expressive 3D representations. However, since there is no prior knowledge on which local features from the two modalities are corresponding, we propose a novel module named

Correspondence-Aware Fusion (CAF) for the fusion process. In essence, it exhaustively computes similarity scores of every local feature pair across the two-modal inputs, and then filters out the low similarity pairs for a sparsified aggregation. The details are described in the following paragraph.

CAF module. The structure of the proposed CAF module is shown in Fig. 3(b). As shown, the CAF module takes two-modal inputs (denoted by X and Y , respectively) which describe the same 3D object and learns to combine them into a compact joint representation. For ease of description, assuming X and Y contain N_X and N_Y local features, respectively, where each local feature is a D -dimensional vector. In other words, $X \in \mathbb{R}^{N_X \times D}$ and $Y \in \mathbb{R}^{N_Y \times D}$. Similar to Self-Attention [37], the CAF module also includes three elements: the query, the key, and the value. The query is estimated based on the modality X , while the key and value are computed based on the other modal input Y . In our design, we implement a multi-head version for the CAF, since it allows us to further explore local relations among different representation subspaces. Concretely, based on the two-modal inputs X and Y , we first apply linear layers to project them parallelly in order to obtain a sequence of H tuples, which are denoted by $[(Q_1, K_1, V_1), (Q_2, K_2, V_2), \dots, (Q_h, K_h, V_h), \dots, (Q_H, K_H, V_H)]$, where (Q_h, K_h, V_h) represents corresponding input tuple for h -th head in the form (query, key, value). The query $Q_h \in \mathbb{R}^{N_X \times D_H}$ is calculated based on X while the key $K_h \in \mathbb{R}^{N_Y \times D_H}$ and value $V_h \in \mathbb{R}^{N_Y \times D_H}$ are based on Y . Empirically, $D = H \times D_H$. Then, we use a submodule named Threshold Fusion (TF) to collect cues from V_h based on the correlations between Q_h and K_h . Mathematically, it first computes the relation or correspondence scores by taking dot product of local feature at each position:

$$\omega_{t,z} = Q_{h,t}^T K_{h,z}, \quad (3)$$

where $\omega_{t,z}$ represents the relation score between t -th position in Q_h and z -th position in K_h . *sigmoid* function is further employed to squash the relation scores into range (0,1). Since smaller scores mean less related local regions across the two modalities, a threshold function is used to filter out them and retain salient corresponding local features:

$$\alpha_{t,z} = \delta(\sigma(\omega_{t,z}), \beta), \quad (4)$$

where $\delta(\cdot)$ represents the threshold function, $\sigma(\cdot)$ represents the *sigmoid* function taking the form $\sigma(x) = \frac{1}{1+\exp(-x)}$, and β represents the threshold value. The analysis on the impact of the threshold β will be presented in section 4. Finally, we collect local features from V_h based on the scores to enhance t -th local features of Q_h in a weighted average manner:

$$G_{h,t} = \frac{\sum_{z=1}^{N_Y} \alpha_{t,z} V_{h,z}}{\sum_{z=1}^{N_Y} \alpha_{t,z} + \epsilon}, \quad (5)$$

where ϵ is set to 1e-5 to avoid division by zero in practice. After obtaining all the outputs from the multi-head branches, we concatenate them along the head dimension, *i.e.*, $G = [G_1, G_2, \dots, G_H]$, where $G \in \mathbb{R}^{N_X \times D}$. It should be noted that the resulting features can be interpreted as re-representation of the local features in X with local features in Y . We also add a residual link to combine the two-modal representations together by element-wise summation:

$$G_{out} = \text{FC}(G) + Q, \quad (6)$$

where FC is the fully connected layer, and $Q = [Q_1, Q_2, \dots, Q_H]$. Finally, The combined representation is fed into two fully connected layers, and a pooling layer which can be max/mean pooling layer is further employed to aggregate G_{out} into a compact one:

$$\mathbf{g}_{YX} = \text{pool}(\text{FC}(G_{out})), \quad (7)$$

where \mathbf{g}_{YX} represents the aggregated two-modal representation by enhancing X with Y . Above we have demonstrated that the representations of X can be improved by collecting cues selectively from Y . However, it is worth mentioning that we can perform representation enhancement in both directions by simply choosing one modality for the query and the other modality for the key and value alternately. Therefore, in the same way, it is easy to obtain the enhanced features in the other direction, denoting by \mathbf{g}_{XY} . Such a bidirectional strategy can integrate the local features of X and Y in a more interactive way.

Specifically, in our framework, we first set X and Y to local point and multi-view features, respectively, which gives us Point-View CAF¹. Then we switch X and Y , which gives us View-Point CAF². The goal of Point-View CAF is to enhance the local point features by exploiting local multi-view features, while View-Point CAF performs feature enhancement in the other direction. Lastly, we insert the Point-View and View-Point CAF modules into our CAP-Net to fuse the local features of the two-modal inputs of the same scale level in a hierarchical manner. Recall that we have obtain a hierarchy of local features for the two modalities, respectively. For each hierarchical level l , we end up with two enhanced representations with View-Point and Point-View CAF modules, which are denoted by $\mathbf{g}_{vp,l}$ and $\mathbf{g}_{pv,l}$, respectively. We then concatenate the outputs of different scales from L View-Point CAF and Point-View CAF modules, respectively:

$$\begin{cases} \mathbf{g}_{vp} = \mathbf{g}_{vp,1} \circledast \mathbf{g}_{vp,2} \circledast \dots \circledast \mathbf{g}_{vp,L} \\ \mathbf{g}_{pv} = \mathbf{g}_{pv,1} \circledast \mathbf{g}_{pv,2} \circledast \dots \circledast \mathbf{g}_{pv,L} \end{cases}, \quad (8)$$

¹We follow DGCNN and implement the pooling layer by concatenating max-pooling and mean-pooling layers.

²We follow MVCNN and apply the max-pooling operation to the features.

Finally, the global view features \mathbf{g}_v and global point features \mathbf{g}_p are combined with the above \mathbf{g}_{vp} and \mathbf{g}_{pv} together by concatenation after being projected through FC layers respectively, which is written as:

$$\mathbf{g}_{final} = \text{FC}(\mathbf{g}_v) \circ \text{FC}(\mathbf{g}_{vp}) \circ \text{FC}(\mathbf{g}_{pv}) \circ \text{FC}(\mathbf{g}_p). \quad (9)$$

Based on it, a network with three fully connected layers are used to make a prediction on the category for the given 3D object. We use cross entropy loss to train our model.

4. Experiments

4.1. Datasets and Evaluation Metrics

We evaluate our framework on 3D object classification and retrieval tasks. Comprehensive experiments are done on popular 3D shape benchmarks, *i.e.*, ModelNet40 and ModelNet10. The ModelNet40 dataset includes 12,311 CAD models divided into 40 categories. Among them, 9,842 models are used for training and the rest 2,468 are for testing. The ModelNet10 dataset is another popular 3D object dataset, which consists of 4,899 3D models in 10 categories. The training set and testing set have 3,991 and 908 models, respectively. For the classification task, Overall Accuracy (OA) and Accuracy Average Class (AAC) are reported. For the retrieval task, mean Average Precision (mAP) is reported.

4.2. Implementation Details

In our experiments, we follow the same preprocessing scheme as PVRNet [48], which uniformly samples 1,024 points and projects 12 views for each 3D model. The base feature extractors for the two modalities, *i.e.*, DGCNN-EConv and Alex-Conv, are initialized by the pretrained DGCNN and MVCNN like PVRNet. In our experiments, D is 256, and the resulting three scale feature maps for the multi-view images are of size $256 \times 6 \times 6$, $256 \times 4 \times 4$ and $256 \times 2 \times 2$, respectively.

For optimization, we first fix the parameters of Alex-Conv and DGCNN-EConv, and train the fusion layers with a Learning Rate (LR) of $1e-2$ and a momentum of 0.9 for training stability. The LR is decayed by a factor of 0.5 every 3 epochs. After 6 epochs, we set the LR to $1e-3$ and fine-tune the whole model. The LR is decayed by a factor of 0.5 every 10 epochs. For the retrieval experiments, the penultimate layer output, which is 256-dimensional, is used as the descriptor for each 3D shape.

4.3. Comparison with the State-of-the-Arts

We first compare our method with representative state-of-the-art methods on the popular 3D shape benchmarks (*i.e.*, ModelNet10 and ModelNet40) covering 3D object classification and retrieval. The following uni-modal based methods are included: 3D shapeNets [41],

Table 1. Classification and retrieval results on the ModelNet40 and ModelNet10 datasets. *Vx.*, *Im.*, *Pt.* and *Pn.* represent voxels, view images, point clouds and panorama-views, respectively. “-” represents unknown)

Methods	Input	ModelNet40		ModelNet10	
		OA	mAP	OA	mAP
3D shapeNets [41]	<i>Vx.</i>	77.3%	49.2%	83.5%	68.3%
VRN [4]	<i>Vx.</i>	91.3%	-	93.6%	-
DeepPano [35]	<i>Pn.</i>	77.6%	76.8%	85.5%	84.2%
MVCNN [36]	<i>Im.</i>	89.9%	80.2%	-	-
GVCNN [11]	<i>Im.</i>	93.1%	84.5%	-	-
SeqViews [13]	<i>Im.</i>	93.4%	89.1%	94.8%	91.4%
3D2SeqViews [12]	<i>Im.</i>	93.4%	90.8%	94.7%	92.1%
PointNet [31]	<i>Pt.</i>	89.2%	-	-	-
PointNet++ [32]	<i>Pt.</i>	90.7%	-	-	-
DGCNN [40]	<i>Pt.</i>	92.2%	81.6%	-	-
FusionNet [17]	<i>Vx., Im.</i>	90.8%	-	93.1%	-
PVNet [47]	<i>Pt., Im.</i>	93.2%	89.5%	-	-
PVRNet [48]	<i>Pt., Im.</i>	93.6%	90.5%	-	-
MMJN [30]	<i>Pt., Im., Pn.</i>	93.8%	89.8%	93.8%	-
Ours	<i>Pt., Im.</i>	94.2%	92.9%	95.9%	94.0%

VRN [4], DeepPano [35], MVCNN [36], GVCNN [11], SeqViews [13], 3D2SeqViews [12], PointNet [31], PointNet++ [32], DGCNN [40]. We also select representative multi-modal based methods for comparison, and these competitors are: FusionNet [17], PVNet [47], PVRNet [48], MMJN [30]. The detailed results are summarized in Table 1.

As shown in Table 1, on the ModelNet40 dataset, the proposed method can reach 94.2% in OA for 3D object classification and 92.9% in mAP for 3D object retrieval, which clearly outperforms existing state-of-the-art uni-modal based methods. In the classification task, compared with VRN which performs the best on learning from voxels, we improve upon it by 2.9% in OA. Our method also yields much better results than those point-cloud-based methods. For instance, we improve PointNet and PointNet++ by 5.0% and 3.5% in OA, respectively. Compared with the more powerful DGCNN which is based on EdgeConv, we achieve 2.0% improvements in OA. When compared with MVCNN which learns from multi-view images, we gain improvements of 4.3% in OA. 3D2SeqViews, which effectively aggregates sequential views using attention mechanism, has the best performance on classification task, reaching 93.4% in OA. Compared with it, we increase the OA by 0.8%. The compared results indicate that fusing different modalities of 3D objects leads to better 3D representations. The comparison results with other multi-modal based methods are very valuable. Compared with FusionNet, significant performance gains of 3.4% in OA are obtained. PVNet and PVRNet both focus on how to fuse the point cloud and multi-views, while PVRNet obtains relatively better performance, reaching 93.6% in OA. However, compared with it, we obtain improvements of 0.6% in OA. MMJN is the recent state-of-the-art multi-modal based

method, and we improve upon it by 0.4% in OA. When it comes to 3D object retrieval, the improvements over state-of-the-art methods are more significant. It is worth mentioning that the MVCNN has adopted metric learning over the learned representation to boost the retrieval performance, while we directly take the representations from our framework as the descriptor for 3D object retrieval. However, When compared with MVCNN, we significantly surpass it by 12.7% in mAP. 3Ds2SeqViews obtains the best mAP, reaching 90.8%. We improve upon it by 2.1%. Among the multi-modal based methods, PVRNet is the current state-of-the-art method, and reaches 90.5% in mAP. Compared with it, we gain an improvement of 2.4%. MMJN also obtains a strong performance with 89.8% in mAP, and we improve upon it by over 3%.

On the ModelNet10 dataset, the proposed method once again demonstrates its superiority on both 3D object classification and retrieval tasks. In the classification task, our method obtains 95.9% OA, which outperforms the unimodal based methods, namely SeqViews and 3D2SeqViews, by 1.1% and 1.2%, respectively. More importantly, our method also obtains strong improvements over the multi-modal based methods. Compared with FusionNet and MMJN, our method increases the OA by 2.8% and 2.1%, respectively. In the retrieval task, encouragingly, our method has reached 94.0% in mAP. When compared with SeqViews, we improve upon it by 2.6% in mAP. 3D2SeqViews is another state-of-the-art method and achieves 92.1% in mAP. We outperform it by 1.9%.

4.4. Discussions

In this subsection, we give an in-depth analysis on the proposed CAP-Net. ModelNet40 is employed for all our ablation experiments for convenience.

Influence of fusion strategies. Table 3 compares our method with other baseline fusion strategies. “Late Fusion” represents fusion method by simply concatenating the global features from the point cloud and multi-view data. “Our DeepConcat” represents fusion by concatenating the hierarchy of the local features from the two modalities. As shown, simply concatenating global features of the two modalities can improve over using only one modality on classification task. However, compared with it, our DeepConcat improves upon it by 1.1% in AAC and 1.0% in OA, which proves the benefits of fusion with local features. More importantly, our CAP-Net succeeds to increase its OA from 93.6% to 94.2% and the AAC from 91.5% to 92.3%, which suggests the benefits of exploiting the local spatial relations of the two modalities in the fusion process.

Influence of different scale combinations. Table 3 studies the effects of different scale combinations. We can observe that with a single scale, the model can already obtain strong performance, reaching 93.8% and 91.2% in OA and

Table 2. Influence of fusion strategies

models	OA	ACC
Point Cloud Model	92.2%	90.2%
Multi-View Model	89.9%	87.6%
Late Fusion	92.6%	90.8%
Our DeepConcat	93.6%	91.5%
Our CAP-Net	94.2%	92.3%

Table 3. Influence of different scale combinations

combinations	OA	ACC
scale 1	93.8%	91.2%
scale 1, 2	94.0%	91.6%
scale 1, 2, 3	94.2%	92.3%

AAC, respectively. With more scale features being incorporated, better performance can be obtained. With all the three scales, we obtain the best results, beating the model using the single scale features by 0.4% and 1.1% in OA and AAC, respectively. These results indicate that more informative features are produced by fusing multi-scale features, since richer relations are exploited.

Influence of β . The threshold β is used to select salient cross-modal correspondences for the fusion process. To investigate its effects, we set it to 0, 0.1, 0.3, 0.5, 0.7, 0.9, respectively. Particularly, $\beta = 0$ means not applying threshold to the scores. As shown in Table 4, when we increase β from 0 to 0.3, better performance is obtained. However, further increasing it leads to the performance drop. The best classification performance is obtained when we set β to 0.3, which reaches 94.21% in OA and 92.28% in ACC. While the best retrieval performance is obtained when β is set to 0.1, reaching 93.03%. We assume that if the threshold is too small, then the fused features contain too much redundant information, hurting the fusion efficacy. However, too large value may filter out much valuable information, thus reducing capacity of the fused features. Appropriate value for threshold (0.1~0.3 in our case) benefits the fusion process.

Influence of k . Table 5 shows the impacts of nearest neighbor number k within the SGP layers. As shown, setting the nearest neighbor numbers for each point to 20 gives us the best performance, reaching 94.21% in OA and 92.28 in ACC for classification and 92.93% for retrieval. It is interesting that further increasing k does not lead to better performance. We assume that too many neighbors may contaminate the local information of each point, while fewer neighbors are not sufficient to describe the local geometric information of each point.

Influence of H . Table 6 presents the performance of our CAP-Net with different number of heads in the CAF modules. As shown, with the number of heads increasing, we observe steady improvements in terms of all the evaluation metrics. We believe that with more heads the module can learn richer associations between the two modalities. The best results are obtained when we set H to 8, reach-

Table 4. Influence of β

β	OA	ACC	mAP
0	93.80%	92.00%	92.85%
0.1	94.00%	92.13%	93.03%
0.3	94.21%	92.28%	92.93%
0.5	93.84%	91.59%	92.91%
0.7	93.72%	91.62%	92.64%
0.9	93.60%	91.52%	92.60%

Table 5. Influence of k

k	OA	ACC	mAP
5	93.52%	90.86%	92.30%
10	93.64%	91.75%	92.58%
15	93.96%	91.72%	92.69%
20	94.21%	92.28%	92.93%
25	94.00%	91.49%	92.72%
30	94.00%	91.81%	92.81%

Table 6. Influence of the head numbers in the CAF modules

H	OA	ACC	mAP
1	93.64%	90.76%	92.53%
2	93.68%	91.12%	92.69%
4	93.88%	91.50%	92.42%
8	94.21%	92.28%	92.93%
16	93.88%	91.34%	92.92%

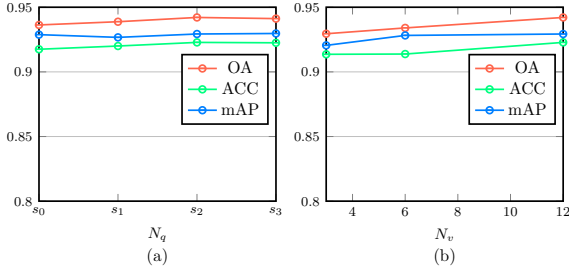


Figure 4. Influence of (a) the number of sampled points and (b) the number of views on the model performance

ing 94.21% in ACC and 92.93% in mAP. However, when H goes beyond 8, the performance gets saturated.

Influence of N_q . To study the impacts of the sampled point numbers N_q by FPS in the three SGP layers, we first conduct experiments by setting N_q in the three SGP layers to be (128, 64, 32) (denoted as s_0) as the base sampled point numbers. Then we double the sampled points in all the SGP layers progressively three times (denoted as s_1, s_2, s_3 , respectively) and re-run the experiments. As shown in Fig. 4(a), the best classification results are achieved when the sampled point numbers are (256, 128, 64). However, further increasing them leads to inferior results. For retrieval, the best performance is achieved when we set the sampled point numbers to (128, 64, 32). Generally, our model is robust to the sampled point numbers in the SGP layers to some extent.

Influence of N_v . Fig. 4(b) studies the influence of the num-

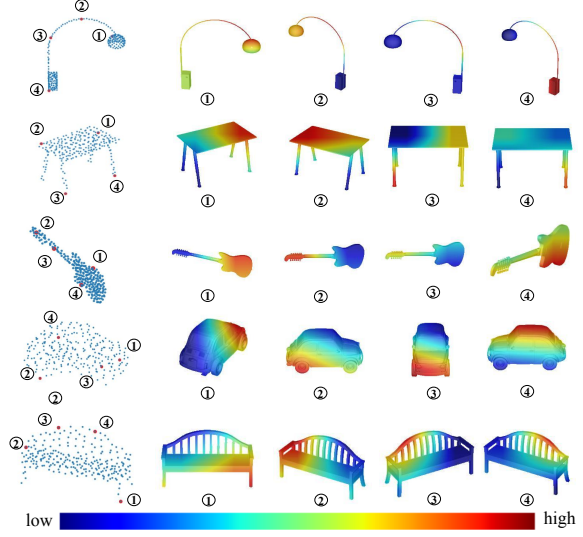


Figure 5. Visualization of the correspondence scores learned by the proposed model

ber of views N_v for each 3D object. We vary N_v to be 3, 6, 12 and then conduct experiments to see its impacts. As shown, more views lead to better performance. Specifically, for classification task, more steady improvements in ACC and OA are observed when the number of views increases. However, for retrieval, the growth rate of mAP gets smaller after the number of views is beyond 3. These results indicate that the classification task benefits more from more view images.

Complexity Analysis. Table 7 compares the complexity of our CAP-Net with the state-of-the-art method PVRNet [48]. As shown, the proposed CAP-Net has $2.8\times$ fewer parameters, while still outperforms PVRNet [48] by a clear margin. Moreover, our CAP-Net also reduces the FLOPs by 8G when the mini-batch size is 16. These results demonstrate the high efficiency of our CAP-Net.

Visualization. Fig. 5 visualizes the correspondence scores learned by our CAP-Net for fusing the two-modal inputs. For simplicity, four points are first selected from the point cloud, and then their local correspondence scores over the four view images are visualized. It can be observed that CAP-Net is highly effective at associating the point features with semantically similar part in the view images.

5. Conclusions

In this paper, we have investigated the effects of fusing point cloud and multi-view data based on their local features. A novel module named Correspondence-Aware Fusion (CAF) is proposed to fuse the two modalities by exploiting their salient local spatial correspondences, which are derived by applying threshold to their correspondence scores. With this module, we construct a framework named

Table 7. Architecture comparison with PVRNet on ModelNet40

Methods	Parameters	FLOPs	OA	mAP
PVRNet [48]	70M	171G	93.6%	90.5%
Ours	25M	163G	94.2%	92.9%

Correspondence-Aware Point-view Fusion Net (CAP-Net) which works in a bidirectional and hierarchical manner in order to fully leverage their local spatial relations. We have shown that the framework is able to obtain significant improvements over existing methods. In the future, we are interested in applying the CAF module to fuse more modalities of 3D objects such as voxels and meshes to explore its generality.

References

- [1] Mathieu Aubry, Ulrich Schlickewei, and Daniel Cremers. The wave kernel signature: A quantum mechanical approach to shape analysis. In *Proc. ICCV Workshop*, pages 1626–1633, 2011. 2
- [2] Song Bai, Xiang Bai, Zhichao Zhou, Zhaoxiang Zhang, and Longin Jan Latecki. Gift: A real-time and scalable 3d shape search engine. In *Proc. CVPR*, pages 5023–5032, 2016. 2
- [3] Song Bai, Zhichao Zhou, Jingdong Wang, Xiang Bai, Longin Jan Latecki, and Qi Tian. Ensemble diffusion for retrieval. In *Proc. ICCV*, pages 774–783, 2017. 2
- [4] Andrew Brock, Theodore Lim, James M Ritchie, and Nick Weston. Generative and discriminative voxel modeling with convolutional neural networks. *Proc. NeurIPS Workshop*, 2016. 6
- [5] Ding-Yun Chen, Xiao-Pei Tian, Yu-Te Shen, and Ming Ouhyoung. On visual similarity based 3d model retrieval. In *Comput Graph Forum*, pages 223–232, 2003. 2
- [6] Guoxian Dai, Jin Xie, and Yi Fang. Siamese cnn-bilstm architecture for 3d shape representation learning. In *Proc. IJ-CAI*, pages 670–676, 2018. 2
- [7] Carlos Esteves, Yinshuang Xu, Christine Allen-Blanchette, and Kostas Daniilidis. Equivariant multi-view networks. *Proc. ICCV*, 2019. 2
- [8] Yi Fang, Jin Xie, Guoxian Dai, Meng Wang, Fan Zhu, Tiantian Xu, and Edward Wong. 3d deep shape descriptor. In *Proc. CVPR*, pages 2319–2328, 2015. 2
- [9] Yutong Feng, Yifan Feng, Haoxuan You, Xibin Zhao, and Yue Gao. Meshnet: mesh neural network for 3d shape representation. In *Proc. AAAI*, pages 8279–8286, 2019. 2
- [10] Yifan Feng, Haoxuan You, Zizhao Zhang, Rongrong Ji, and Yue Gao. Hypergraph neural networks. In *Proc. AAAI*, pages 3558–3565, 2019. 2
- [11] Yifan Feng, Zizhao Zhang, Xibin Zhao, Rongrong Ji, and Yue Gao. Gvcnn: Group-view convolutional neural networks for 3d shape recognition. In *Proc. CVPR*, pages 264–272, 2018. 2, 6
- [12] Zhizhong Han, Honglei Lu, Zhenbao Liu, Chi-Man Vong, Yu-Shen Liu, Matthias Zwicker, Junwei Han, and CL Philip Chen. 3d2seqviews: Aggregating sequential views for 3d global feature learning by cnn with hierarchical attention aggregation. *IEEE TIP*, 2019. 6
- [13] Zhizhong Han, Mingyang Shang, Zhenbao Liu, Chi-Man Vong, Yu-Shen Liu, Matthias Zwicker, Junwei Han, and CL Philip Chen. Seqviews2seqlabels: Learning 3d global features via aggregating sequential views by rnn with attention. *IEEE TIP*, pages 658–672, 2018. 2, 6
- [14] Rana Hanocka, Amir Hertz, Noa Fish, Raja Giryes, Shachar Fleishman, and Daniel Cohen-Or. Meshcnn: a network with an edge. *ACM TOG*, page 90, 2019. 2
- [15] Xinwei He, Tengting Huang, Song Bai, and Xiang Bai. View n-gram network for 3d object retrieval. In *Proc. ICCV*, pages 7515–7524, 2019. 2
- [16] Xinwei He, Yang Zhou, Zhichao Zhou, Song Bai, and Xiang Bai. Triplet-center loss for multi-view 3d object retrieval. In *Proc. CVPR*, pages 1945–1954, 2018. 2
- [17] Vishakh Hegde and Reza Zadeh. Fusionnet: 3d object classification using multiple data representations. *arXiv preprint arXiv:1607.05695*, 2016. 2, 6
- [18] Asako Kanezaki, Yasuyuki Matsushita, and Yoshifumi Nishida. Rotationnet: Joint object categorization and pose estimation using multiviews from unsupervised viewpoints. In *Proc. CVPR*, pages 5010–5019, 2018. 2
- [19] Michael Kazhdan, Thomas Funkhouser, and Szymon Rusinkiewicz. Rotation invariant spherical harmonic representation of 3 d shape descriptors. In *Symposium on geometry processing*, pages 156–164, 2003. 2
- [20] Marcel Körtgen, Gil-Joo Park, Marcin Novotni, and Reinhard Klein. 3d shape matching with 3d shape contexts. In *The 7th central European seminar on computer graphics*, pages 5–17, 2003. 2
- [21] Alex Krizhevsky, Ilya Sutskever, and Geoffrey E Hinton. Imagenet classification with deep convolutional neural networks. In *Proc. NeurIPS*, pages 1097–1105, 2012. 3
- [22] Biao Leng, Liqun Li, and Zheng Qin. Made: a composite visual-based 3d shape descriptor. In *International Conference on Computer Vision/Computer Graphics Collaboration Techniques and Applications*, pages 93–104, 2007. 2
- [23] Biao Leng, Cheng Zhang, Xiaochen Zhou, Cheng Xu, and Kai Xu. Learning discriminative 3d shape representations by view discerning networks. *IEEE TVCG*, 2018. 2
- [24] Jiaxin Li, Ben M Chen, and Gim Hee Lee. So-net: Self-organizing network for point cloud analysis. In *Proc. CVPR*, pages 9397–9406, 2018. 2
- [25] Xinhai Liu, Zhizhong Han, Yu-Shen Liu, and Matthias Zwicker. Point2sequence: Learning the shape representation of 3d point clouds with an attention-based sequence to sequence network. In *Proc. AAAI*, pages 8778–8785, 2019. 2
- [26] Yongcheng Liu, Bin Fan, Shiming Xiang, and Chunhong Pan. Relation-shape convolutional neural network for point cloud analysis. In *Proc. CVPR*, pages 8895–8904, 2019. 2

- [27] Chao Ma, Wei An, Yinjie Lei, and Yulan Guo. Bv-cnns: Binary volumetric convolutional networks for 3d object recognition. In *Proc. BMVC*, page 4, 2017. 2
- [28] Daniel Maturana and Sebastian Scherer. Voxnet: A 3d convolutional neural network for real-time object recognition. In *Proc IROS*, pages 922–928, 2015. 1, 2
- [29] Sanjeev Muralikrishnan, Vladimir G. Kim, Matthew Fisher, and Siddhartha Chaudhuri. Shape unicode: A unified shape representation. In *Proc. CVPR*, June 2019. 3
- [30] Weizhi Nie, Qi Liang, An-An Liu, Zhendong Mao, and Yangyang Li. Mmjn: Multi-modal joint networks for 3d shape recognition. In *Proc. ACM MM*, pages 908–916. ACM, 2019. 3, 6
- [31] Charles R Qi, Hao Su, Kaichun Mo, and Leonidas J Guibas. Pointnet: Deep learning on point sets for 3d classification and segmentation. In *Proc. CVPR*, pages 652–660, 2017. 1, 2, 6
- [32] Charles Ruizhongtai Qi, Li Yi, Hao Su, and Leonidas J Guibas. Pointnet++: Deep hierarchical feature learning on point sets in a metric space. In *Proc. NeurIPS*, pages 5099–5108, 2017. 2, 3, 6
- [33] Dietmar Saupe and Dejan V Vranić. 3d model retrieval with spherical harmonics and moments. In *Joint Pattern Recognition Symposium*, pages 392–397, 2001. 2
- [34] Nima Sedaghat, Mohammadreza Zolfaghari, Ehsan Amiri, and Thomas Brox. Orientation-boosted voxel nets for 3d object recognition. *Proc. BMVC*, 2017. 2
- [35] Baoguang Shi, Song Bai, Zhichao Zhou, and Xiang Bai. Deeppano: Deep panoramic representation for 3-d shape recognition. *IEEE SPL*, pages 2339–2343, 2015. 2, 6
- [36] Hang Su, Subhransu Maji, Evangelos Kalogerakis, and Erik Learned-Miller. Multi-view convolutional neural networks for 3d shape recognition. In *Proc. ICCV*, pages 945–953, 2015. 1, 2, 6
- [37] Ashish Vaswani, Noam Shazeer, Niki Parmar, Jakob Uszkoreit, Llion Jones, Aidan N Gomez, Łukasz Kaiser, and Illia Polosukhin. Attention is all you need. In *Proc. NeurIPS*, pages 5998–6008, 2017. 2, 5
- [38] Chu Wang, Marcello Pelillo, and Kaleem Siddiqi. Dominant set clustering and pooling for multi-view 3d object recognition. *Proc. BMVC*, 2017. 2
- [39] Peng-Shuai Wang, Yang Liu, Yu-Xiao Guo, Chun-Yu Sun, and Xin Tong. O-cnn: Octree-based convolutional neural networks for 3d shape analysis. *ACM TOG*, page 72, 2017. 2
- [40] Yue Wang, Yongbin Sun, Ziwei Liu, Sanjay E Sarma, Michael M Bronstein, and Justin M Solomon. Dynamic graph cnn for learning on point clouds. *ACM TOG*, page 146, 2019. 2, 3, 6
- [41] Zhirong Wu, Shuran Song, Aditya Khosla, Fisher Yu, Linguang Zhang, Xiaoou Tang, and Jianxiong Xiao. 3d shapenets: A deep representation for volumetric shapes. In *Proc. CVPR*, pages 1912–1920, 2015. 2, 6
- [42] Saining Xie, Sainan Liu, Zeyu Chen, and Zhuowen Tu. Attentional shapecontextnet for point cloud recognition. In *Proc. CVPR*, pages 4606–4615, 2018. 2
- [43] Cheng Xu, Zhaoqun Li, Qiang Qiu, Biao Leng, and Jingfei Jiang. Enhancing 2d representation via adjacent views for 3d shape retrieval. In *Proc. ICCV*, October 2019. 2
- [44] Yifan Xu, Tianqi Fan, Mingye Xu, Long Zeng, and Yu Qiao. Spidercnn: Deep learning on point sets with parameterized convolutional filters. In *Proc. ECCV*, pages 87–102, 2018. 2
- [45] Jiancheng Yang, Qiang Zhang, Bingbing Ni, Linguo Li, Jinxian Liu, Mengdie Zhou, and Qi Tian. Modeling point clouds with self-attention and gumbel subset sampling. In *Proc. CVPR*, pages 3323–3332, 2019. 2
- [46] Ze Yang and Liwei Wang. Learning relationships for multi-view 3d object recognition. In *Proc. ICCV*, pages 7505–7514, 2019. 2
- [47] Haoxuan You, Yifan Feng, Rongrong Ji, and Yue Gao. Pvnnet: A joint convolutional network of point cloud and multi-view for 3d shape recognition. In *Proc. ACM MM*, pages 1310–1318, 2018. 1, 2, 4, 6
- [48] Haoxuan You, Yifan Feng, Xibin Zhao, Changqing Zou, Rongrong Ji, and Yue Gao. Pvrnet: Point-view relation neural network for 3d shape recognition. In *Proc. AAAI*, pages 9119–9126, 2019. 1, 2, 4, 6, 8, 9
- [49] Tan Yu, Jingjing Meng, and Junsong Yuan. Multi-view harmonized bilinear network for 3d object recognition. In *Proc. CVPR*, pages 186–194, 2018. 2
- [50] Zizhao Zhang, Haojie Lin, Xibin Zhao, Rongrong Ji, and Yue Gao. Inductive multi-hypergraph learning and its application on view-based 3d object classification. *IEEE TIP*, pages 5957–5968, 2018. 2
- [51] Hengshuang Zhao, Li Jiang, Chi-Wing Fu, and Jiaya Jia. Pointweb: Enhancing local neighborhood features for point cloud processing. In *Proc. CVPR*, pages 5565–5573, 2019. 2